Soft Exoskeleton Mimics Human Cough for Assisting the Expectoration Capability of SCI Patients

Yan Zhang, Ziqi Wang, Qinggang Ge, Zongyu Wang, Xiangjie Zhou, Shaohang Han, Weidong Guo, Yuru Zhang, *Senior Member, IEEE*, and Dangxiao Wang, *Senior Member, IEEE*

***Abstract*— This paper describes the design of a bionic soft exoskeleton and demonstrates its feasibility for assisting the expectoration function rehabilitation of patients with spinal cord injury (SCI). *Methods:* A human–robot coupling respiratory mechanic model is established to mimic human cough, and a synergic inspire–expire assistance strategy is proposed to maximize the peak expiratory flow (PEF), the key metric for promoting cough intensity. The negative pressure module of the exoskeleton is a soft "iron lung" using layer-jamming actuation. It assists inspiration by increasing insufflation to mimic diaphragm and intercostal muscle contraction. The positive pressure module exploits soft origami actuators for assistive expiration; it pressures human abdomen and bionically "pushes" the diaphragm upward. *Results:* The maximum increase in PEF ratios for mannequins, healthy participants, and patients with SCI with robotic assistance were 57.67%, 278.10%, and 124.47%, respectively. The soft exoskeleton assisted one tetraplegic SCI patient to cough up phlegm successfully. *Conclusion:* The experimental results suggest that the proposed soft exoskeleton is promising for assisting the expectoration ability of SCI patients in everyday life scenarios. *Significance:* The proposed soft exoskeleton is promising for advancing the application field of rehabilitation exoskeletons from motor functions to respiratory functions.**

***Index Terms*— Soft robotics, exoskeletons, rehabilitation robotics.**

Manuscript received August 2, 2021; revised February 24, 2022; accepted March 18, 2022. Date of publication March 28, 2022; date of current version April 18, 2022. This work was supported by the National Natural Science Foundation of China under Grant 82172553. *(Yan Zhang and Ziqi Wang contributed equally to this work.) (Corresponding authors: Dangxiao Wang; Qinggang Ge.)*

This work involved human subjects or animals in its research. Approval of all ethical and experimental procedures and protocols was granted by the Institutional Review Board of Clinical Trials Identifier under Approval No. IRB00006761- M2020520.

Yan Zhang, Ziqi Wang, Xiangjie Zhou, Shaohang Han, Weidong Guo, and Yuru Zhang are with the State Key Laboratory of Virtual Reality Technology and Systems, Beihang University, Beijing 100191, China.

Qinggang Ge and Zongyu Wang are with the Department of Intensive Care Unit, Peking University Third Hospital, Beijing 100191, China (e-mail: qingganggelin@126.com).

Dangxiao Wang is with the State Key Laboratory of Virtual Reality Technology and Systems, and the Beijing Advanced Innovation Center for Biomedical Engineering, Beijing 100191, China, and also with the Peng Cheng Laboratory, Nanshan 518066, China (e-mail: hapticwang@buaa.edu.cn).

This article has supplementary downloadable material available at https://doi.org/10.1109/TNSRE.2022.3162578, provided by the authors.

Digital Object Identifier 10.1109/TNSRE.2022.3162578

I. Introduction

THE estimated number of people with spinal cord injuries (SCIs) worldwide has exceeded three million [1]–[3]. SCI patients are associated with a 50% reduction in respiratory function, which leads to the incapability to clear an airway through coughing [4]–[7]. Respiratory complications including respiration failure, pneumonia, and atelectasis caused by hypoventilation and secretion retention have been considered as the primary determinant factor of increased mortality rate [8]–[10]. In addition, according to World Population Prospects 2019, 1 of every 6 people in the world will be 65 years old or older by 2050, and respiratory diseases such as chronic pneumonia affect 15 in 100 seniors [11]–[13]. The limited number of rehabilitation places cannot meet the requirements of the rising number of patients with expectoration dysfunction. Therefore, a home-used respiration rehabilitation device is expected to bring rehabilitation benefits for more patients.

Secretion clearance is generally used to decrease respiratory complications and improve alveolar ventilation. For the manual thrust method, a therapist provides manual expiratory assistance for patients to increase the peak expiratory flow (PEF) and further cough up secretions; however, this method poses a high technical requirement for a therapist. Medical devices like standard airway suction adopt negative pressure to suction sputum; its high efficiency (no more than 15s) and low-cost (5-10 RMB per operation) have made it the most widely treatment clinically. Mechanical insufflation–exsufflation (MI-E) secretion clearance can facilitate cough by alternately changing human oral pressure for nearly three minutes and increasing PEF above 180 L/min [14]. Even though the existing medical devices possess advantages such as simplicity of use, limited efforts are made to improve the safety, portability and usability of secretion clearance devices.

Soft wearable exoskeletons have demonstrated the potential to assist people in regaining various motor functions such as hand movement [15]–[20] and limb movement [21]–[24]. However, these soft devices have not yet been used in the field of respiratory rehabilitation.

When designing the cough-assistive exoskeleton, the fundamental scientific question is to understand the biological

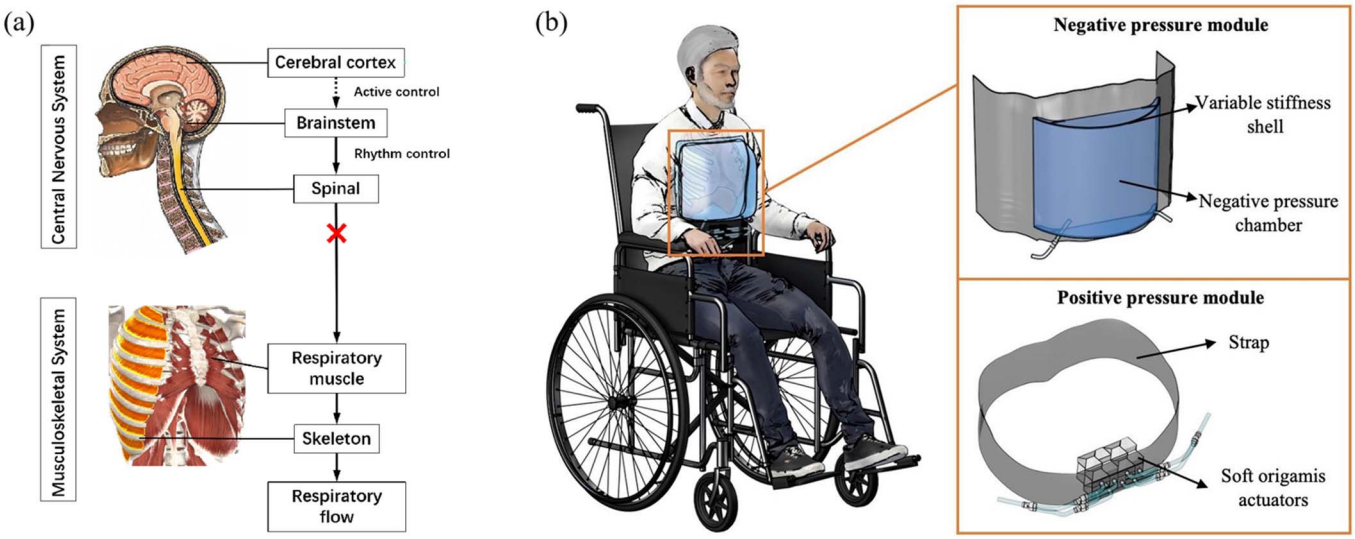

Fig. 1. Bionic concept design of a soft exoskeleton for SCI patients. (a) Injury to the high-level spinal cord affects the spinal nerves that innervate respiratory muscles and produces flaccid paralysis of the respiratory muscles used to perform forceful cough. (b) SCI patient in a wheelchair wears the soft exoskeleton. The negative pressure module consists of a variable stiffness shell and a negative pressure chamber. The positive pressure module is composed of soft origami actuators and a restraining strap.

process of the human cough and to find a bionic robotic-actuated solution for mimicking the process. Clinical studies indicate that the degree of secretion clearance is mainly determined by the cough density, and the PEF has been proven to be one of the convincing quantitative indicators of cough intensity [25]–[29]. Thus, the exoskeleton aims to significantly increase the PEF to cough up phlegm in a bionic, noninvasive assistive way.

To attain soft, portable, and daily-use purposes, the engineering challenges for developing this type of soft exoskeleton include determining how to leverage soft materials and fabrication advances to innovate robotic actuation and control, achieving the purpose of respiratory action assistance. The key innovations of our exoskeleton include the following three aspects.

First, a human–robot coupling respiratory mechanic model is established to quantify the human–robot coupling respiration mechanism and maximize the expiratory flow rate. The model provides a theoretical basis for bionic robotic design, which leads to a novel human–robot coordinated control strategy to control different modules of the exoskeleton acting sequentially and precisely to mimic the human cough process.

Second, to assist inspiration, we develop a negative pressure module. The module assists the patient's chest cavity expansion by way of vacuum adsorption through a sealed negative pressure chamber covered by a variable stiffness shell. Exploiting the layer jamming sheet (LJS) principle, we propose a soft and thin shell enclosing a sufficiently large volume chamber. With variable stiffness capability, the "soft" shell can switch to be "stiff" enough to withstand the high negative pressure within the vacuum chamber. For assisting expiration, we develop a positive pressure module to squeeze the epigastrium and assist diaphragm movement upward. To ensure the thin size of the exoskeleton, soft origami-inspired actuators are mounted adjacent to the bottom line of the processus xiphoideus for abdominal thrust. We present a "fiber-reinforced double-layer method" for fabricating soft origami units capable with both a sufficient deployment ratio and high force output. With a control strategy based on model prediction, the soft origami units produce pulsed-like forces exceeding 200N within 200ms. The origami-inspired soft actuators satisfy the requirements of abdomen thrust including the thin size, the high output force, and the quick response.

Third, the proposed soft exoskeleton opens the novel application for using the exoskeleton technique in the field of respiration rehabilitation. It confers physiological advantages and fuels the hope of assisting the expectoration of SCI patients or the expectoration dysfunction of elderly people with minimal side effects, as well as breakthroughs for the limitation of use location and time in terms of its noninvasive, lightweight, and portable features.

II. Fundamentals of Soft Exoskeleton

SCI patients cannot generate a forceful cough because of injured spinal nerves that innervate the respiratory muscles as shown in Fig.1(a). In this study, a soft cough-assistive exoskeleton is proposed to assist the movement of respiration muscles of SCI patients and to achieve a high PEF to cough up phlegm in an everyday life scenario. The schematic diagram of soft exoskeleton is shown in Fig.1(b).

A. Biorobotic Concept Design Based on Human Cough Mechanism

The process of a cough is shown in Fig. 2 to clarify the cough-related muscle [30]. First, the external intercostal muscles contract and the diaphragm moves downward, resulting in inspiration behavior. The expiratory forces generated by the abdominal muscles against the closed glottis lead to a rapid pressure increase in the lung. Subsequently, the glottis suddenly opens, causing the high-pressure air in the lungs to

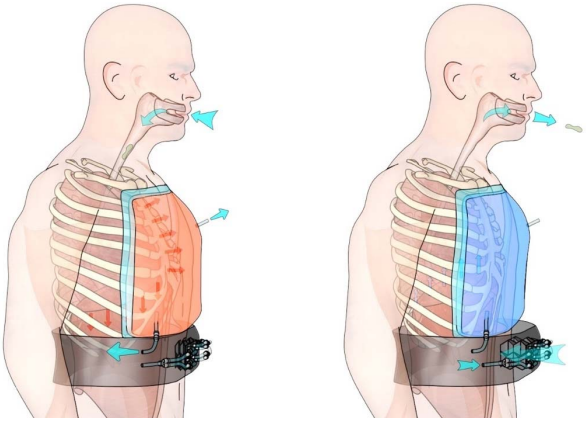

Fig. 2. The negative pressure module "lifts" the ribs up and outward to assist inspiration by generating negative pressure around a human chest. The positive pressure module squeezes the abdominal muscles and helps the upward movement of diaphragm, thus promoting coughing up phlegm by the fast airflow from inside to outside.

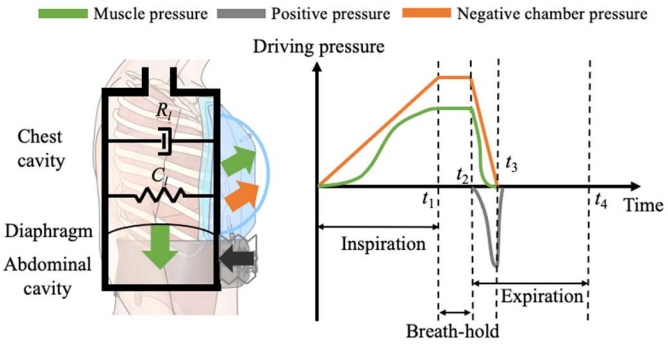

Fig. 3. Human–robot coupling respiration mechanical model. The model couples robotic-assistive pressure to the lung dynamics. A driving pressure pattern including the total muscle pressure, negative pressure, and positive pressure is shown to investigate the dynamic relationship between the combined effort of the respiration muscles and the robotic assistance and lung system.

spray out. Thereby, the phlegm in the trachea is coughed up from the mouth. The mechanism demonstrates that the expiratory muscles, especially the abdominal muscles, including both the rectus abdominis (the anterior wall of the abdomen) and the external obliques (lateral anterior abdomen), play a significant role in a forceful cough. In addition, inspiratory muscles, mainly composed of the diaphragm (at the bottom of the chest) and the intercostal muscles (between the ribs), can increase the insufflation and lung elastic recoil, which further promotes cough tensity.

SCI patients are usually faced with a weak cough due to paralyzed respiratory muscles. The weakness degree of the respiratory muscles is closely related to the level and completeness of the SCI, and respiratory impairment is more severe in high cervical injuries. According to the classification using the International Standards for Neurological Classification of Spinal Cord Injury (ISNCSCI) developed by the American Spinal Injury Association (ASIA) [31], SCIs above C5 and lower thoracic and lumbar nerve injuries result in the weakness of the intercostal and abdominal muscles. For SCIs of C3-C4, phrenic nerve injuries cause impaired diaphragm function [9]. Thus, the dysfunction of both the inspiratory and expiratory muscles results in a weak cough.

To make the dysfunctional respiration muscles "regain" their motor function and further generate a forceful PEF in a noninvasive way, we propose an exoskeleton. The bionic concept design of soft exoskeleton is proposed based on the impaired cough mechanics of SCI patients. Two modules are designed to mimic both inspiratory and expiratory muscles: (1) The negative pressure module, which evacuates the pressure between the exoskeleton and the patient's chest to help the ribs move up and outward to increase lung volume. The negative pressure module mimics the effect of contraction of both the diaphragm and the external intercostal muscles. (2) The positive pressure module, which provides an impact on the epigastrium to pressure the abdomen cavity and speed up the expiratory flow rate. In addition, the increased pressure within the abdominal cavity "pushes" the diaphragm upward biconically.

B. Human–Machine Coupling Respiration Mechanic Model

To quantify the flow dynamic characteristics and parameterize the robotic pressure profile, a human–robot coupling respiration mechanism is proposed. The strategy is to first neglect the inertial effects in that the mass terms are considered negligible when compared with the viscous and elastic terms. Then the robot acting forces are modeled by compensating for the muscle and driving respiration capability beyond the innate physiological levels. Finally, the bionic robotic actuation and control method is proposed.

The human–robot coupling respiration mechanic model and its equivalent one-order mechanical representation are shown in Fig. 3. The lung cavity is depicted as a compliant structure with volume that is connected to a robot system. The driving forces (pressure) and their acting patterns including robotic forces and muscle forces are contained in the mechanic model. The mechanical representation includes the parameters of compliance and viscous resistance and the acting forces, which vary during the respiratory cycle. In the model, the airway flow is selected as the system output because it is the indicator for evaluating cough intensity and it can be measured under different circumstances, thereby providing quantified metrics for the model's accuracy.

The respiratory dynamic equation can be modeled with

$$\begin{cases} R_l \dot{V}_l + V_l / C_l = P_a + P_m + P_r \\ P_r = P_{rn} + P_{rp} \end{cases} \tag{1}$$

where V_l represents the lung volume, R_l denotes the lung and airway resistance in the range of 1–3 $cmH_2o/(L{\cdot}s)$ for person without lung and chest diseases, C_l is the lung and chest compliance in the range of 0.05–0.1 L/ cmH_2o for person without lung and chest diseases [32]–[36]. P_a, P_m, and P_r denote the pressures of the atmosphere, total respiration muscle, and robot assistance. P_{rn} and P_{rp} are the pressures of the negative and positive modules. The atmospheric pressure is the zero reference for all pressure measurements ($P_a = 0$). On the left-hand side of (1), the first term represents the viscous resistance forces, and the second term represents the

elastic forces. The terms on the right-hand side of the (1) alternatively represent the driving forces. The sign of the driving forces is positive if the forces function to expand the lung volume and negative if the forces compress the volume.

According to Jodat's model [37], the total muscle driving force for quiet breathing can be presented as a trigonometric function [38]–[42]. For SCI patients cough process, it can be seen as inhalation and passive exhalation because of their paralyzed abdominal muscle; thus we apply the respiration model to simulate cough process of SCI patient. Moreover, before the glottis opens, there is one more breath-holding step for coughing; therefore, the muscle forces for keeping the breath held are taken into consideration as follows:

$$P_m = \begin{cases} K_1[1-\cos(\pi t/t_1)], & (0 < t \le t_1) \\ 2K_1, & (t_1 < t \le t_2) \\ K_1[1+\cos(\pi\ (t-t_2+t_1)/t_1-\pi)], & (t_2 < t \le t_3) \\ 0, & (t_3 < t \le t_4) \end{cases} \tag{2}$$

where K_1 characterizes the maximum for the muscle pressure, α_1 and α_2 are the decisive factors that determine the profile of the muscle pressure, t_1, t_2, and t_4 denote the times at the end of inspiration, breath-hold, and expiration, and t_3 is the time when the expiratory flow is reduced to 0. SCI patients usually face weakness or paralysis of the expiratory muscles. Thus, the expiration is assumed to be a passive process similar to resting breathing.

In addition to muscle driving, the exoskeleton also drives the rib cage and diaphragm. The negative pressure module acting on the rib cage is termed the robotic negative pressure (P_{rn}) and expressed as

$$P_{rn} = \begin{cases} K_n t, & (0 < t \le t_1) \\ K_n t_1, & (t_1 < t \le t_2) \\ -K_n t_1 (t-t_3)/(t_3-t_2), & (t_2 < t \le t_3) \\ 0, & (t_3 < t \le t_4) \end{cases} \tag{3}$$

where K_n represents the growth rate of the negative pressure.

The positive pressure module mimics the expiratory muscles that are recruited during forced breathing like a cough to reduce the abdominal cavity and to compress lung air. According to the cough mechanism, the expiratory forces against the closed glottis will increase lung pressure sharply. Thus, the origami actuators need to produce synchronized compressive forces along with the output forces of the expiratory muscles. Because the mechanical behavior of soft origamis is nonlinear, we use the trigonometric function to model its acting forces. A model of the robotic acting forces is as follows:

$$P_{rp} = \begin{cases} 0, & (0 < t \le t_2) \\ K_p V_o / C_l [1-\cos(\pi (t-t_2)/(t_3-t_2)], & (t_2 < t \le t_3) \\ 0, & (t_3 < t \le t_4) \end{cases} \tag{4}$$

where V_o denotes the inflated volume of the origami actuators, and K_p represents the pressure coefficient of the soft origamis.

C. Design and Characterization of Negative Pressure Module

A negative pressure module is placed around the chest wall to incorporate the whole rib cage and assist the inspiratory muscles contraction by intermittently applying a subatmospheric pressure. The applied negative pressure aims to overcome the resistance of the human skin–muscle–skeleton system to assist chest expansion. To avoid interference during the working process and to ensure the chamber volume during the working process, the impedance boundary determination criteria of the negative pressure module is proposed as follows: For any given negative pressure chamber pressure, the sum of the height of the human chest x_c and the deformation of the shell depressed by the atmospheric pressure x_j should be less than the original height of the shell.

Compared with traditional noninvasive negative pressure ventilation devices that use a stiff shell, the variable stiffness architecture of a negative pressure module was proposed to improve the wearability of the soft exoskeleton. To fulfill this goal, one major challenge for designing the shell of the negative pressure module is to meet the conflicting requirements between the resting state and the working state. In the resting state, the shell should be as soft as a piece of exosuit, so that patients can feel light and comfortable. In the working state, the shell should become as stiff as a "rigid shell", and thus sustain its original shape and withstand the negative pressure within the vacuum chamber. In one word, an ideal shell should be sufficiently flexible in the resting state and provide a high stiffness in the working state.

Layer jamming actuators have the capability of simulating variable stiffness whereas allowing for constructing the thin and lightweight form factors of a device [43]–[45]. The principle of a layer jamming mechanism is to control the friction between the layers of a thin material by evacuating the air pressure between the layers [46]. In this study, we leverage the concept of layer jamming to solve the conflicting design for the negative pressure module.

As shown in Fig. 1(b), the negative pressure module is composed of a variable stiffness shell using a layer jamming sheet (LJS) and a sealed negative pressure chamber to assist rhythmic thoracic expansion. For the purpose of the compact structure, an arch-shaped shell is selected (the design detail is shown in Note S1). Two supporting planes of the shells can provide certain support for the top surface not to collapse. The physical prototype is shown in Fig. 4 and the fabrication method is elaborated on in Note S2.

Fig. 4 and movie S1 demonstrate that the LJS shell exhibits tunable stiffness. To further demonstrate the characteristic of the LJS shell, Fig. 5 shows the deformation of the center point of the arch-shaped shell related to the applied negative pressure within the chamber for both the unjammed and jammed states.

When two layers of the stacked soft sand strip coils begin to bend, it evolves through three regimes: the pre-slip, translation, and full-slip regimes [46]. In pre-slip, there is no slip of the layers, and the structure manifests a high bending stiffness. Thus, the deflection can be neglected. The longitudinal shear stress of each point of the contact interface of the two layers

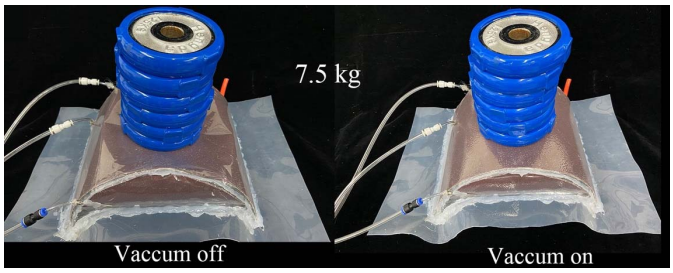

Fig. 4. When the vacuum is off, the LJS shell has low bending stiffness. When the vacuum is on, the structure has high bending stiffness. Calibrated dumbbells (1.25 kg for a single dumbbell) are used to test the load capacity of the LJS shell.

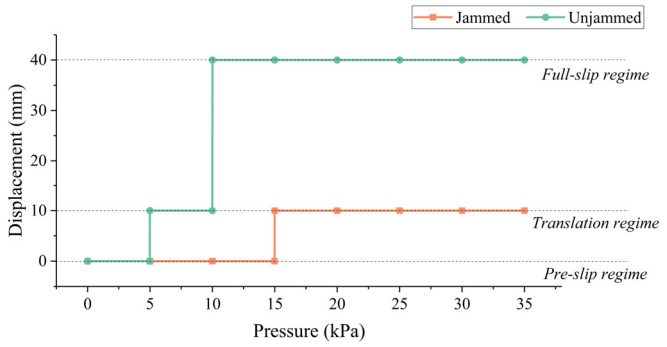

Fig. 5. Mechanical behavior of LJS shell. When the vacuum is on, the layers squeeze each other and the maximum static friction value is increased, leading to a larger pre-slip and translation regime. The LJS will not enter to full-slip when the negative pressure is smaller than 35 kPa, which results in a better loading endurance performance. When the vacuum is off, the structure behaves plastically and experiences three deformation regimes.

is equal and the stress increases along with the time in pre-slip. When the longitudinal shear stress is greater than the static friction stress, the structure enters the translation regime in which the layers begin to slip. In this regime, the maximum deformation is 10 mm because of the relatively stable structure of the arch shape of the LJS shell. With the increasing pressure of the chamber, the structure enters the full-slip regime in which all points between the layers slip along their interfaces. Accordingly, the bending stiffness decreases significantly when slip occurs because the energy is dissipated to friction between the layers to a great extent.

To ensure reliability and avoid the collapse of the LJS during the working state, it is preferred for the LJS under extreme pressure to work in the *pre-slip* or *translation* regimes to ensure high stiffness.

D. Design and Characterization of Positive Pressure Module

Considering the fact that the expiratory muscles (abdominal muscles) provide most of the forces during a cough, the positive pressure module is designed to squeeze abdominal muscles. This exploits a combination of soft actuators and a restraining strap (Velcro). The actuators are constrained within the unstretchable strap to expand inward when actuated (Fig. 1(b)). To meet the requirement of expiration assistance, determination requirements of impedance boundary of the positive pressure module need to be fulfilled: The tensile stiffness of the restraint belt material should be much greater than the stiffness of the actuator to ensure that the total length between the robot and the human body remains unchanged. The frictional force provided by the restriction strap should be greater than the interaction force of the soft actuator and the human body. The impedance of the soft actuator is greater than that of the abdominal cavity of the human body to limit the deformation of the actuator toward the human body.

To achieve a large height variation, the Yoshimura origami cylinder actuator is adopted and adapted in this study because of its strengths in symmetric growth in the height direction [47]. The large friction coefficient between two layers of Velcro plays a role in fixation. The length of the strap can be adjusted to accommodate the epigastric perimeters of different people. The origami-inspired actuators are in the middle position of the connection line between the xiphoid and the navel, covering the upper abdomen of the human body. The actuators are composed of eight soft actuators side by side, with four in each row. The actuators recoil back and keep a contracted state in the nonworking state.

The geometric parameters of soft Yoshimura origami (Y-ori) are shown in Note S3 and refer Fig. S2 for details [48], [49]. The soft origami can be unfolded and stretched, achieving dual-mode morphing similar to the actuator made by Woongbae [50]. However, the soft actuator fabricated by Woongbaes elastomer casting method termed the “layer stacking method” can only output forces below 3 N. Therefore, it cannot provide a sufficiently high impact force (exceeding 200 N) to squeeze the human abdomen effectively.

Here, we present a novel monolithic fabrication method, termed the “fiber-reinforced double-layer method,” for the three-dimensional (3D) architecture of a soft origami unit that can generate a high force output and an excellent pressure bearing capability. In this method, the lost-wax process [51]–[53] is used for the inner mold to make monolithic forming possible. Furthermore, the relatively large prefolding angle makes it possible to attach fibers to silicone to improve the pressure bearing capacity and limit radial deformation [54]–[56].

Detailed fabrication processes are illustrated in Fig. 6. First, 3D printed molds for an inner wax mold with a rod, external mold, and outer mold are prepared. First, molten wax is poured into the cavity through the gate (Fig. 6(a)) and then cured at room temperature to form a Y-ori wax core with an embedded carbon fiber rod to enable precise positioning in the following steps. In particular, a rod with a screw thread is chosen to prevent the unacceptable rotation and improve the positioning accuracy of the wax core in the following processes. Then the solid wax Y-ori is wrapped by two parts of the external molds and accurately positioned by the rod and the located boss. The elastomer is poured into the outer mold and cured to form the inner silicone with the Y-ori wax core inside (Fig. 6(b)). As shown in Fig. 6(c), fibers are attached to the silicone core manually using inextensible Kevlar thread in a left-right symmetrical double helix configuration. Then the outer silicone skin is fabricated using the outer mold,

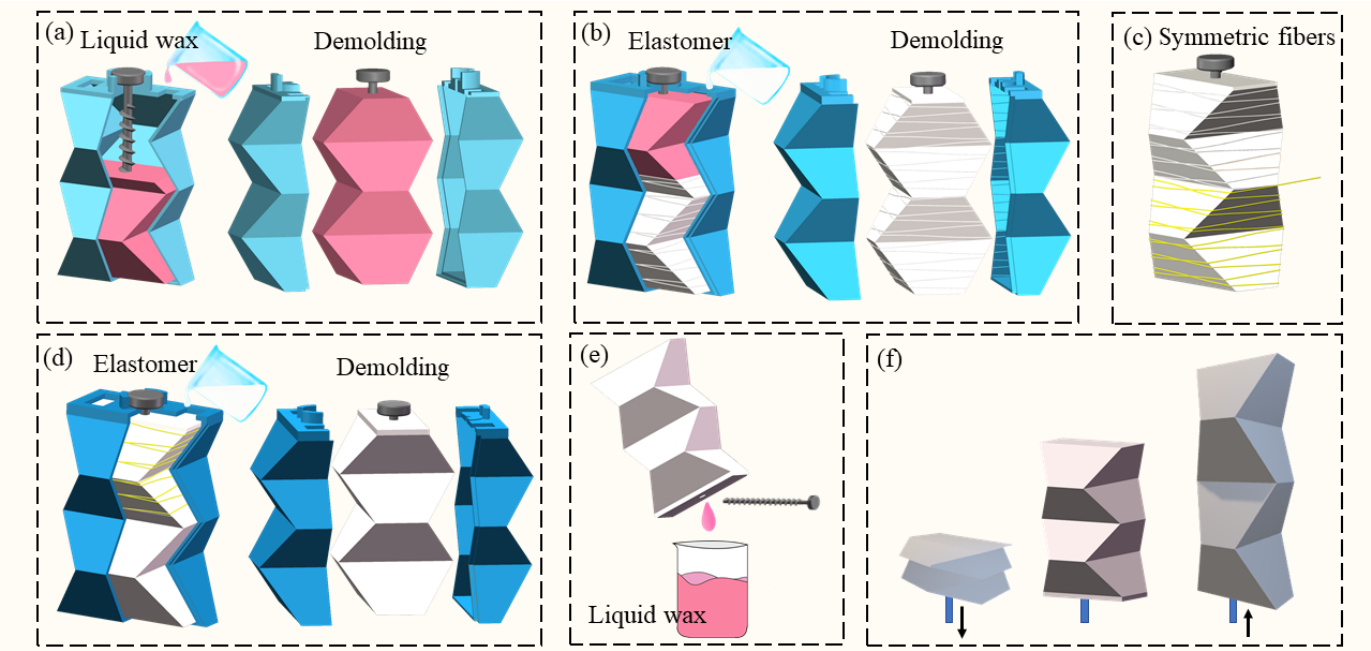

Fig. 6. Fiber-reinforced, double-layered integrated fabrication method. In this method,the lost-wax process is used to achieve monolithicformation and increase the air tightness of the actuator. Furthermore, two sets of symmetrical fibers are adopted to improve the output forces and limit radial deformation. The final soft origami is not only deployable but also stretchable.

as presented in Fig. 6(d), similar to Fig. 6(b). After a similar curing process for the outer silicone skin, the actuator is put into hot water at nearly 60°C to melt the inner wax core (the melting point of paraffin wax is 50°C–60°C). Then the carbon fiber rod is extracted from the actuator when the wax core is totally molten. Subsequently, the liquid wax drips out of the silicone because of the effect of gravity, as shown in Fig. 6(e). Finally, a soft elastomeric actuator is formed with the novel monolithic fabrication method, as displayed in Fig. 6(f).

To accurately control the exoskeleton for rapid abdominal thrust during the coughing process, it is necessary to characterize the performance of the soft origami actuator. The fabricated prototype has a compact initial configuration, and it demonstrates its strength in axial elongation, as shown in Fig. 7.

The result demonstrates that the soft origami has a 400% elongation that can satisfy the height requirement during abdominal thrust. The output force is also investigated. A full description of the characterization studies is provided in Note S4. The force characterization experiments demonstrate that an output force exceeding 200 N can be delivered from the actuators (Fig. 8, and Movie S2).

In addition to high output forces, the time response of soft origami is another key indicator. To meet the rapid air response control while ensuring the safety of the soft origami actuator, we design a control strategy based on the model prediction (Fig. S4(a) and Note S4). Our approach is to increase the pneumatic source pressure to increase the inflation rate of the pneumatic system and use an electromagnetic valve combined with an electronic circuit for the valve opening time control. Before validating the time responses of soft origami, we set the initial height of the soft origami to 8.4 cm, set

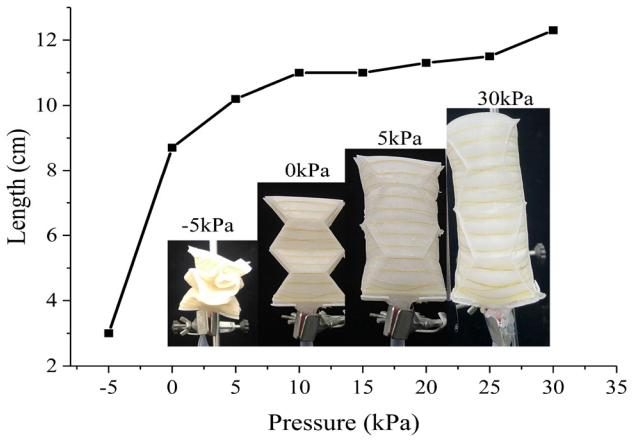

Fig. 7. Length change and morphing behaviors of soft origami in response to inner pressure. The inset images indicate the pre-folded, original, unfolded, and stretched states of the soft stretchable origami.

the number of actuators to eight, and optimize the supply tube system. The reason for this is that the response time varies with the number of actuators and the damping of the supply system, which makes it difficult to simultaneously satisfy the required response time and the higher output force. Furthermore, the force profiles of soft origamis under 100 kPa, 130 kPa, and 150 kPa in 200 ms are analyzed to validate the time response. It can be concluded that the amplitude of the output force of the soft origamis increases slightly with the increase of the pneumatic source pressure. The inflation time decreases and both the force keeping time and the deflation time increase with the increase of the pneumatic source pressure (Fig. 8).

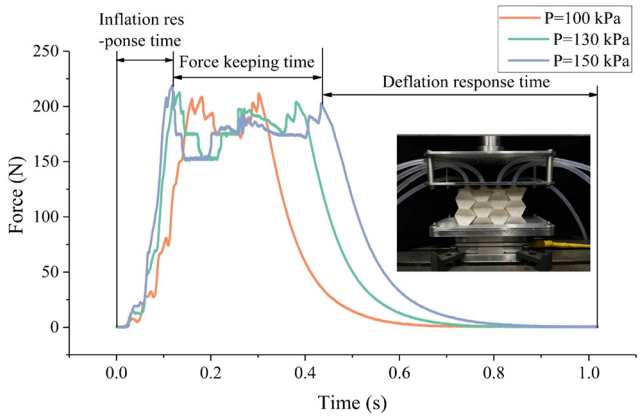

Fig. 8. The experimental scenario of mechanical testing of soft origamis. The valve opening time is equal to 200 ms.

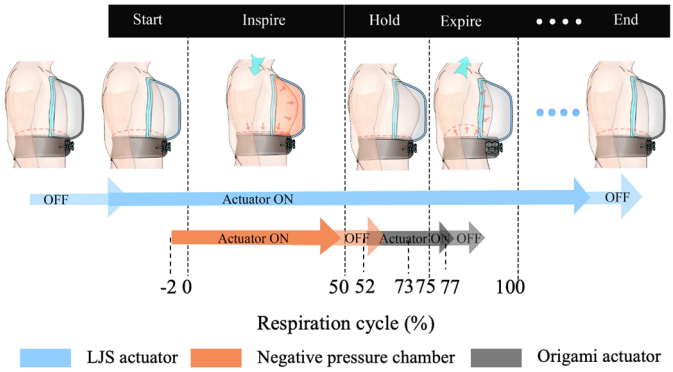

Fig. 9. Timing control strategy of the soft exoskeleton and the human–robot coordinated control strategy. The total duration of one respiration cycle is approximately 4 s, the inspiration phase occupies 50% of the cough cycle, amounting to 2 s, and the breath-holding phase lasts for 1 s. The negative pressure chamber begins to deflate 100 ms earlier than inspiration. The soft origamis start to inflate 100 ms earlier than the glottis opens and stop with the PVT (approximately 100 ms).

E. Human–Robot Coordinated Control Strategy

The actuation of the exoskeleton is performed by an integrated pneumatic source including a positive control system and two negative control systems. The components of control system are elaborated in Note S5.

To make the robotic assistance more effective, the action sequence of both the positive and negative pressure modules of the soft exoskeleton is proposed based on the proposed coupling model (Fig. 9). At the start of a cough assistance working cycle, the jamming shell is deflated to its extreme negative pressure, and it continues to be stiff during the whole cough cycle. The inspiration phase is set to occupy 50% of the cough cycle to obtain a deep inspiration. Thus, the negative pressure chamber functions during the whole inspiration. The negative pressure chamber needs to return to its original pressure within the breath holding phase so that the residual pressure does not affect the expiratory phases.

The impact force is exerted on the human abdomen by the inflation of the soft origami when the glottis opens. If the impact force of soft origami is too early, the human glottis may open in advance, which makes the pressure in the lung and the expiratory flow rate decrease sharply. However, the impact force will not contribute to an increase of the airway flow rate if it is applied on the abdomen after the glottis opens because the lung is no longer a closed cavity and because the decrease of the lung volume cannot make an increase of flow. Therefore, the soft origami needs to start inflation before the exact moment when the human glottis opens and the output impact force occurs within the time that the expiratory flow reaches the maximum peak velocity time (PVT). Thus, considering the air response of soft origamis and the PVT value of a human, the soft origamis should start to inflate 100 ms earlier than the glottis opens and then deflate at the PVT time.

To meet the output force requirements of different modules of the exoskeleton, the allowable control parameter ranges are analyzed based on the characterization experimental results shown in Fig. 8. For the positive module, the pneumatic source pressure can vary between 100 and 150 kPa, with 100 kPa being the minimum pressure setting that reaches the minimum air pressure limit for solenoid valves. For the negative pressure module, the jamming shell is jammed at −76 kPa (pneumatic negative pressure source) to lock its original shape and to withstand the differential pressure inside and outside the shell. For the negative pressure chamber, its pressure is decided by both the deflation rate and the air leakage rate. Therefore, to obtain a maximal lung insufflation and avoid any influence on a patients blood pressure or cause of discomfort, the pneumatic negative pressure source of the chamber can be varied within minus 30 kPa to adapt to different patients.

Asynchrony is a common problem for both ventilated and manual assistive techniques. It results in not only a significant reduction of the effectiveness but also a risk to the interface of a patients voluntary respiratory action. Therefore, to make the human–robot coordinated process easier and more effective, the synchronization between the exoskeleton and a human during assistive cough needs to be solved.

The glottis needs to stay closed during the breath-holding phase of the cough process, which results in obvious increased intrathoracic pressure and forceful, high-velocity expiration as soon as the glottis opens. Clinical evidence shows that SCI patients retain the motor function of throat muscles to control the glottis opening and closing. Therefore, we design a respiration instruction strategy to achieve synchronized human–robot cooperation.

Different instruction words including inspire, hold, and expire appear on the computer screen in turn, and the patient needs to act synchronously with the given words. The timing control strategy is as follows. The LJS shell is jammed when the exoskeleton starts to work. To maximize a patients lung insufflation, the inspiration time is set to 2 s and the patient is asked to inspire. During this period, the negative pressure chamber is vacuumed and human thoracic expansion is assisted. If “Hold” appears on the screen and continues around 1 s, the patient needs to stop inspiring and voluntarily close his glottis. The positive pressure module begins to inflate approximately 100 ms earlier than the “Expire” instruction appears.

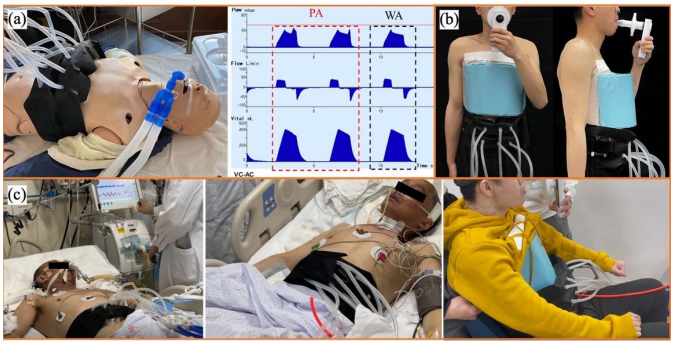

Fig. 10. Experimental setup. (a) Mannequin testing; the mannequin is connected to a ventilator through tracheal intubation to simulate human airflow. The airway flow profile is read directly from the ventilator; PA denotes positive pressure module assistance, and WA denotes without robotic assistance. (b) Healthy participant testing. (c) SCI patient testing: mechanical-ventilated patient, EET-removed patient, home-rehabilitated patient.

III. Rerults

We conduct tests with a mannequin, healthy participants, and SCI patients wearing the soft exoskeleton to validate the robotic effect on the PEF increment (Fig. 10).

Inclusion criteria of participants are described in Note S6. All the 20 healthy participants and the 3 patients are included in the protocol after meeting the criteria and providing written informed consent (Clinical Trials Identifier, IRB00006761-M2020520).

A. Mannequin Testing

Before the experiments in human testing, we first perform mannequin testing to validate and optimize the design and control parameters of the exoskeleton, as well as clarify the influence of robotic assistance on the flow rate. Because the skin of the mannequin is unstrechable, which makes the negative pressure module ineffective, the mannequin experiment only aims to verify the assistive effect of the robotic positive pressure module. In addition, the mannequin lacks an artificial diaphragm. Thus, pressing the epigastrium will not cause the shrinkage of the lung volume as it would in a human. Therefore, the positive pressure module is directly worn on the mannequin chest to validate the robotic assistive effect.

Fig. 10(a) presents the comparison of the respiratory mechanical parameters of the ventilated mannequin with and without robotic assistance. The lung pressure (Paw in Fig. 10(a)) also has a sudden surge before the start of expiration with the thrust of the robotic positive module and the PEF increases obviously.

The effect of the control variables including the pressure and the inflation duration on the PEF are analyzed. The increment of the PEF has an obvious positive correlation relationship with the positive pressure P and the inflation duration of soft origami actuators denoted as t (maximum increase of 57.67% in Fig. 11). When $t \leq 150$ ms and $P \leq 100$ kPa, there is little increase of the PEF, which is mainly the result of the unstable morphing and output for the not-fully expanded origami actuators under this condition. Additionally, the origami actuators

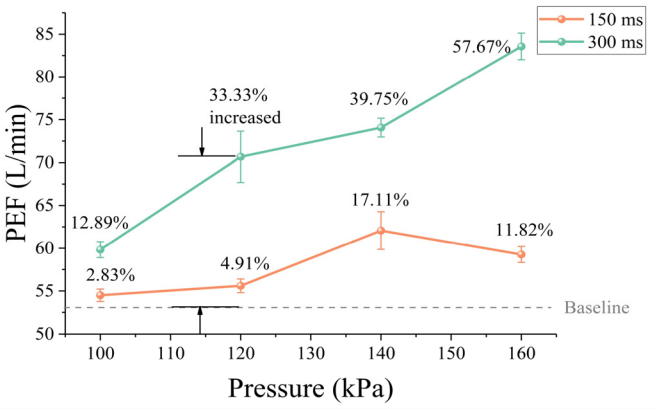

Fig. 11. The PEF has minimal increase (<5% increasing ratio) when t 200 ms and P 200 kPa and the obvious positive correlation with pressure is kept when t = 300 ms.

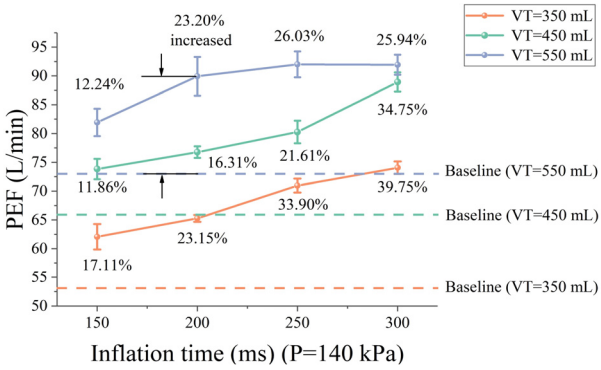

Fig. 12. The PEF increases with the increase of the VT, while the increasing ratio for different VT values remains similar.

reach an unacceptably high risk of explosion when the pressure is greater than 160 kPa, which can likely cause lateral expansion at the fiber restricted areas. Therefore, the ranges of P and t are determined, namely, $100 \text{ kPa} < P \leq 160 \text{ kPa}$ and $150 \text{ ms} < t \leq 300 \text{ ms}$.

Three values of the tidal volume (VT) that are correlated to human heights and weights are analyzed in Fig. 12. The results demonstrate that the value of PEF increases with the increase of the VT. However, the increasing ratio of the PEF with the same control parameters shows no relationship with the VT. Thus, considering the individual differences, the increasing ratio of the PEF with and without robotic assistance is selected as the evaluation index of the robotic cough-assistive effect in this study.

B. Health Participant Testing

The human testing is conducted on healthy participants to validate the effectiveness and the safety of robotic cough assistance before testing on SCI patients. The subjects are first given an overview of the research and told about the risk involved in the measurements. After calibration and familiarization with the system over 3 min to 4 min, the subjects are asked to hold a spirometer to perform the flow rate measurements, as shown in Fig. 10(b).

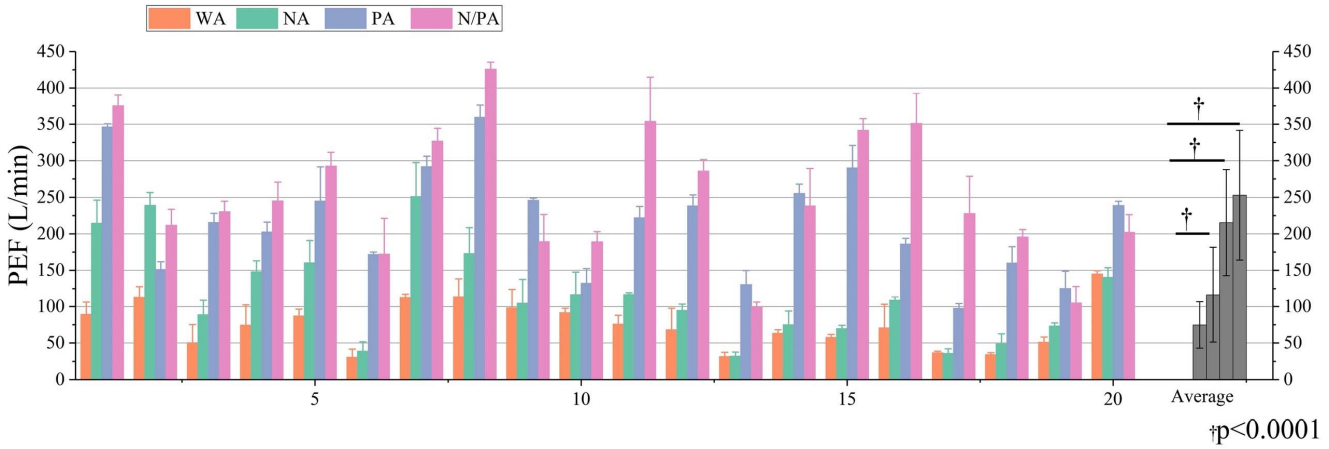

Fig. 13. The PEFunder fourconditions for allparticipants.The bars arethemeans,theerror bars arethe standard deviation,and †denotes thestatistical significance.

To evaluate the contribution of the negative and positive pressure module to increasing the coughing performance as well as their integrated effect, four types of flow measurements including without robotic assistance (WA), negative pressure module assistance (NA), positive pressure module assistance (PA), or negative plus positive pressure module assistance (N/PA) are conducted. The results of normal respiration (i.e., without robotic assistance, WA) are used as the baseline for evaluating the assistance effect of the robot under other three conditions. Each test is repeated three times for every subject.

As shown in Fig.13 and Table S1, with robotic assistance, the PEFs for NA, PA, and N/PA increase significantly compared with those of WA. The average PEFs of the healthy participants for NA, PA, N/PA increase by 50.74 ± 42.36%, 220.21 ± 117.37%, and 278.10 ± 147.28%, respectively. The matched samples t-test shows a significant difference ($p < 0.0001$, $n = 20$).

Note S7 presents the simulation parameter estimation method based on the healthy participant experiments. Fig. S5 shows that the maximum residual between the fitted PEF for the healthy participant results and the calculated PEF based on the proposed coupling respiratory mechanic model is less than 7%, confirming the effectiveness of the theoretical model.

C. SCI Patients Case Study

The effect of the exoskeleton has been validated on three SCI patients with different types of symptoms (Fig. 10(c)). For all the patients, the PEF of the maximum voluntary cough increases significantly with positive pressure module assistance (Fig. 14). The exoskeleton successfully assists one SCI participant with respiration dysfunction to cough up phlegm independently (Movie S3). Additionally, the PEF increment and the phlegm-cough-up differ for the state of SCI. Thus, an in-depth analysis is given.

The first patient (male, 55, C6-C7, A level) is mechanically ventilated via an orotracheal cannula. The vital volume of the patient is set in advance through a ventilator, which makes it difficult to validate the effectiveness of the negative pressure part. The values of the PEF are collected directly by the ventilator. The results demonstrate that for the single

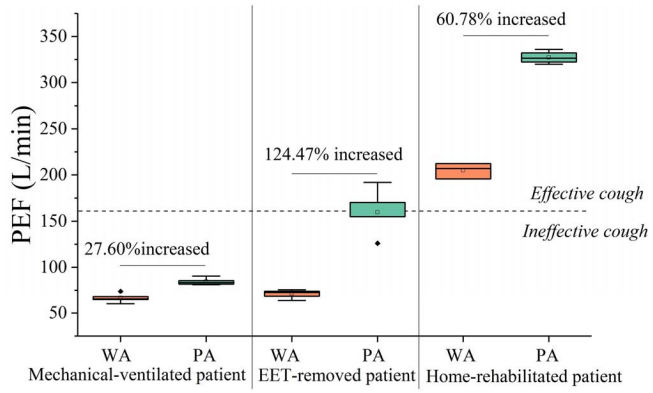

Fig. 14. Comparison of the PEF of the SCI patients with different injury levels with and without robotic assistance. For different kinds of SCI patients, the increasing ratios are different. The centerlines show the medians. The box limits indicate the 25th and 75th percentiles.

positive pressure module assistance, the PEF of the patient increases by 27.60% and the maximum value achieved is 90.60 L/min. However, the maximum of the PEF still does not reach the threshold of the PEF for producing an effective cough (160 L/min). The reason for this is that although the patient can perform a cough action, the continuously opened glottis makes it difficult for air compression to occur in the lung. Therefore, the mechanically ventilated SCI patient is not applicable for robotic phlegm-cough-up, but the positive module can be applied for abdominal muscles training.

The second patient (male, 52, C4, A level) who has intubation removed for one day has excessive phlegm and a weak cough function after a surgical operation. The patient cannot follow the respiration instruction because of poor consciousness. Thus, the robotic action is manually controlled by the doctor. The PEF of the patient increases by 124.47% and the maximum value achieved is 192.00 L/min, which exceeds the effective cough threshold. Movie S3 shows that the patient coughs up the phlegm independently with positive pressure assistance.

For the home-rehabilitated patient (male, 32, C5, B level) who can cough independently but strenuously after two years of rehabilitation, four conditions including WA, NA, PA, and

N/PA are conducted to validate the assistive effect of both the negative and positive pressure modules as well as their synergy effect. The PEF is measured by a spirometer. The PEF increasing ratios for NA, PA, and N/PA are 20.00%, 60.78%, and 35.22%, respectively, and the maximum of the PEF reaches 336 L/min. The patient reports that the negative pressure module can apparently assist inspiration and the positive module can strengthen the cough effectively. However, it is difficult for the patient to cooperate with both the negative and positive pressure modules, leading to a relatively small increment of N/PA compared with NA. Additionally, the cough capability of the patient has been partially rehabilitated and the volume of phlegm decreases. The soft exoskeleton presents its potential application in expectoration assistance.

IV. Discussion

The performance of the device is quantitatively compared with the existing devices including Iron Lung, Cuirass, Exovent and pneumobelt, as shown in Table S4 [57]–[61]. Although the proposed soft exoskeleton shows great strength compared with current expectoration devices in terms of noninvasiveness and portability, several aspects of the performance of the soft exoskeleton can be further improved.

First, during the robotic assistance process, patient–robot asynchronization is found to be the most important factor that directly determines the assistive results. The human–robot coordination strategy could be optimized using a series of expectoration–intention detection methods such as a diaphragm electromyogram (EMG) or electroencephalogram (EEG) for better human–robot synchronization and more "intelligent" assistance.

Second, the soft exoskeleton improves cough capability by assisting primary respiration muscles, whereas the accessory inspiratory muscles including the sternomastoid, scalenus anterior muscle, and trapezius, which are located in the neck and back, are not included. It remains to be seen whether assisting other accessory respiratory muscles could be more effective during respiration.

Finally, the optimized design of soft exoskeleton should be directed as follows: 1) The effectiveness of soft origamis assistance will be further improved by changing the actuation direction from perpendicular to diagonally upward. The upward component of the acting forces will help the diaphragm move upward directly during expiration. 2) The wearability of the soft exoskeleton may be improved by making the negative pressure shell more form-fitting. The controllable shape techniques can be combined with layer jamming actuation to make an exosuit with variable shapes and stiffness.

People with COVID-19 are facing respiratory dysfunction including the retention of phlegm, posing an urgent need for respiratory rehabilitated exoskeletons. Additionally, patients with respiratory disorders as well as aging people with degraded respiratory function, could also use the soft exoskeleton to assist coughing and improve respiratory function. The results of this study suggest that embedding similar bionic assistive principles into expectoration or respiratory rehabilitation devices can potentially avoid ventilator-induced lung injury and make the rehabilitation process easier and more comfortable. In the future, a portable soft exoskeleton may further promote wider clinical application.

V. Conclusion

Inspiration–expiration synergy bionic cough assistance presents greater improvement in cough tensity, few side effects, and more comfort than previous expectoration devices. The theoretical human–robot coupling respiratory mechanic model provides new ideas for noninvasive and physiological clinical expectoration treatment. Soft exoskeleton assistance increases the PEF for a mannequin, healthy participants, and SCI patients. The mannequin testing experiment verifies the feasibility of the cough bionic design and determines the robotic control parameters in terms of the PEF increase. The comparison results of healthy participant testing experiment under four conditions quantifiably characterize the assisting principles and the PEF increase for the single negative and positive pressure modules as well as their synergy action. For SCI patients, the result shows that SCI patients who have cough dysfunction can intensify their cough capability using the proposed soft exoskeleton. One EET-removed tetraplegic patient who has excessive phlegm enhances expectoration function with robotic assistance. The SCI patient testing experiments further demonstrate that the positive pressure module squeezes the paralyzed abdominal muscles of SCI patients forcefully and increases the PEF. The positive pressure module of the soft exoskeleton plays the most important role in cough assistance. The negative pressure module of the soft exoskeleton demonstrates the potential in the application in lung function rehabilitation.

References

[1] L. G. Spencer *et al.*, "Global, regional, and national burden of traumatic brain injury and spinal cord injury, 1990–2016: A systematic analysis for the global burden of disease study 2016," *Lancet Neurol.*, vol. 18, no. 1, pp. 56–87, Jan. 2019.

[2] J. H. Badhiwala, J. R. Wilson, and M. G. Fehlings, "Global burden of traumatic brain and spinal cord injury," *Lancet Neurol.*, vol. 18, no. 1, pp. 24–25, Jan. 2019.

[3] A. Singh, L. Tetreault, S. Kalsi-Ryan, A. Nouri, and M. G. Fehlings, "Global prevalence and incidence of traumatic spinal cord injury," *Clin. Epidemiol.*, vol. 6, pp. 309–331, Sep. 2014.

[4] R. Brown, A. F. DiMarco, J. D. Hoit, and E. Garshick, "Respiratory dysfunction and management in spinal cord injury," *Respiratory Care*, vol. 51, no. 8, pp. 853–868, Aug. 2006.

[5] A. B. Jackson and T. E. Groomes, "Incidence of respiratory complications following spinal cord injury," *Arch. Phys. Med. Rehabil.*, vol. 75, no. 3, pp. 270–275, Mar. 1994.

[6] D. J. Berlowitz, B. Wadsworth, and J. Ross, "Respiratory problems and management in people with spinal cord injury," *Breathe*, vol. 12, no. 4, pp. 328–340, Dec. 2016.

[7] G. J. Schilero *et al.*, "Traumatic spinal cord injury: Pulmonary physiologic principles and management," *Clin. Chest Med.*, vol. 39, no. 2, pp. 411–425, Jun. 2018.

[8] J. J. Cragg, F. M. Warner, J. K. Kramer, and J. F. Borisoff, "A Canada-wide survey of chronic respiratory disease and spinal cord injury," *Neurology*, vol. 84, no. 13, pp. 1341–1345, Mar. 2015.

[9] J. T. Hachmann, P. J. Grahn, J. S. Calvert, D. I. Drubach, K. H. Lee, and I. A. Lavrov, "Electrical neuromodulation of the respiratory system after spinal cord injury," *Mayo Clinic Proc.*, vol. 92, no. 9, pp. 1401–1414, Sep. 2017.

[10] M. B. Zimmer, K. Nantwi, and H. G. Goshgarian, "Effect of spinal cord injury on the respiratory system: Basic research and current clinical treatment options," *J. Spinal Cord Med.*, vol. 30, no. 4, pp. 319–330, Jan. 2007.

[11] M. S. Baek, S. Park, J.-H. Choi, C.-H. Kim, and I. G. Hyun, "Mortality and prognostic prediction in very elderly patients with severe pneumonia," *J. Intensive Care Med.*, vol. 35, no. 12, pp. 1405–1410, Dec. 2020.

[12] J.-P. Janssens and K.-H. Krause, "Pneumonia in the very old," *Lancet Infectious Diseases*, vol. 4, no. 2, pp. 112–124, Feb. 2004.

[13] A. M. Fein, "Pneumonia in the elderly: Special diagnostic and therapeutic considerations," *Med. Clinics North Amer.*, vol. 78, no. 5, pp. 1015–1033, Sep. 1994.

[14] E. Servera *et al.*, "Non-invasive management of an acute chest infection for a patient with ALS," *J. Neurol. Sci.*, vol. 209, nos. 1–2, pp. 111–113, May 2003.

[15] H. K. Yap, J. H. Lim, F. Nasrallah, and C. H. Yeow, "Design and preliminary feasibility study of a soft robotic glove for hand function assistance in stroke survivors," *Frontiers Neurosci.*, vol. 11, no. 547, pp. 1–14, Oct. 2017.

[16] P. Polygerinos, K. C. Galloway, E. Savage, M. Herman, K. O. Donnell, and C. J. Walsh, "Soft robotic glove for hand rehabilitation and task specific training," in *Proc. IEEE Int. Conf. Robot. Autom. (ICRA)*, May 2015, pp. 2913–2919.

[17] X. Chen, L. Gong, L. Zheng, and Z. Zou, "Soft exoskeleton glove for hand assistance based on human-machine interaction and machine learning," in *Proc. IEEE Int. Conf. Hum.-Mach. Syst. (ICHMS)*, Sep. 2020, pp. 6–11.

[18] L. Gerez, G. Gao, A. Dwivedi, and M. Liarokapis, "A hybrid, wearable exoskeleton glove equipped with variable stiffness joints, abduction capabilities, and a telescopic thumb," *IEEE Access*, vol. 8, pp. 173345–173358, 2020.

[19] X. Chen *et al.*, "A wearable hand rehabilitation system with soft gloves," *IEEE Trans. Ind. Informat.*, vol. 17, no. 2, pp. 943–952, Feb. 2021.

[20] P. Polygerinos *et al.*, "Towards a soft pneumatic glove for hand rehabilitation," in *Proc. IEEE/RSJ Int. Conf. Intell. Robots Syst.*, Nov. 2013, pp. 1512–1517.

[21] K. A. Witte, P. Fiers, A. L. Sheets-Singer, and S. H. Collins, "Improving the energy economy of human running with powered and unpowered ankle exoskeleton assistance," *Sci. Robot.*, vol. 5, no. 40, p. 9108, Mar. 2020.

[22] B. T. Quinlivan *et al.*, "Assistance magnitude versus metabolic cost reductions for a tethered multiarticular soft exosuit," *Sci. Robot.*, vol. 2, no. 2, p. 4416, Jan. 2017.

[23] Y. Ding, M. Kim, S. Kuindersma, and C. J. Walsh, "Human-in-the-loop optimization of hip assistance with a soft exosuit during walking," *Sci. Robot.*, vol. 3, no. 15, Feb. 2018, Art. no. eaar5438.

[24] L. N. Awad *et al.*, "A soft robotic exosuit improves walking in patients after stroke," *Sci. Transl. Med.*, vol. 9, no. 400, Jul. 2017, Art. no. eaai9084.

[25] S. T. Kulnik, S. S. Birring, J. Hodsoll, J. Moxham, G. F. Rafferty, and L. Kalra, "Higher cough flow is associated with lower risk of pneumonia in acute stroke," *Thorax*, vol. 71, no. 5, pp. 474–475, May 2016.

[26] K. K. Menezes, L. R. Nascimento, L. Ada, J. C. Polese, P. R. Avelino, and L. F. Teixeira-Salmela, "Respiratory muscle training increases respiratory muscle strength and reduces respiratory complications after stroke: A systematic review," *J. Physiotherapy*, vol. 62, no. 3, pp. 138–144, Jul. 2016.

[27] L. Haviv *et al.*, "Using a sniff controller to self-trigger abdominal functional electrical stimulation for assisted coughing following cervical spinal cord lesions," *IEEE Trans. Neural Syst. Rehabil. Eng.*, vol. 25, no. 9, pp. 1461–1471, Sep. 2017.

[28] J. K. Gupta, C.-H. Lin, and Q. Chen, "Flow dynamics and characterization of a cough," *Indoor Air*, vol. 19, no. 6, pp. 517–525, Dec. 2009.

[29] U. Mellies and C. Goebel, "Optimum insufflation capacity and peak cough flow in neuromuscular disorders," *Ann. Amer. Thoracic Soc.*, vol. 11, no. 10, pp. 1560–1568, Dec. 2014.

[30] K. F. Chung and I. D. Pavord, "Prevalence, pathogenesis, and causes of chronic cough," *Lancet*, vol. 371, no. 9621, pp. 1364–1374, Apr. 2008.

[31] F. M. Maynard *et al.*, "International standards for neurological and functional classification of spinal cord injury," *Spinal Cord*, vol. 35, no. 5, pp. 266–274, May 1997.

[32] J. B. West and A. M. Lucks, *West's Respiratory Physiology: The Essentials*, 10th ed. Peking Univ. Med. Press, Beijing, China, 2015.

[33] B. Herlihy, "Respiratory physiology," *Crit. Care Nurse*, vol. 4, no. 5, pp. 58–59, Sep. 1984.

[34] S. P. Rao and S. E. Dicarlo, "Respiratory physiology—Introduction," *Adv. Physiol. Educ.*, vol. 25, no. 2, pp. 55–61, Jun. 2001.

[35] H. S. Harb, N. I. Laz, H. Rabea, and M. E. A. Abdelrahim, "Prevalence and predictors of suboptimal peak inspiratory flow rate in COPD patients," *Eur. J. Pharmaceutical Sci.*, vol. 147, Apr. 2020, Art. no. 105298.

[36] P. J. Heaf and F. J. Prime, "The compliance of the thorax in normal human subjects," *Clin. Sci.*, vol. 15, no. 2, pp. 319–327, May 1956.

[37] R. W. Jodat, J. D. Horgan, and R. L. Lange, "Simulation of respiratory mechanics," *Biophys. J.*, vol. 6, no. 6, pp. 773–785, Nov. 1966.

[38] E. Agostoni, J. E. Chinnock, M. D. B. Daly, and J. G. Murray, "Functional and histological studies of the vagus nerve and its branches to the heart, lungs and abdominal viscera in the cat," *J. Physiol.*, vol. 135, no. 1, pp. 182–205, Jan. 1957.

[39] E. Agostoni and H. Rahn, "Abdominal and thoracic pressures at different lung volumes," *J. Appl. Physiol.*, vol. 15, no. 6, pp. 1087–1092, Nov. 1960.

[40] E. Agostoni, "Mechanics of the pleural space," *Physiol. Rev.*, vol. 52, no. 1, pp. 128–157, Jan. 1972.

[41] E. Agostoni, G. Gurtner, G. Torri, and H. Rahn, "Respiratory mechanics during submersion and negative-pressure breathing," *J. Appl. Physiol.*, vol. 21, no. 1, pp. 251–258, Jan. 1966.

[42] A. W. Sheel and L. M. Romer, "Ventilation and respiratory mechanics," *Comprehensive Physiol.*, vol. 2, no. 2, pp. 1093–1142, Apr. 2012.

[43] D. S. Shah, E. J. Yang, M. C. Yuen, E. C. Huang, and R. Kramer-Bottiglio, "Jamming skins that control system rigidity from the surface," *Adv. Funct. Mater.*, vol. 31, no. 1, pp. 1–8, Sep. 2020.

[44] Y. Zhang, D. Wang, Z. Wang, Y. Zhang, and J. Xiao, "Passive force-feedback gloves with joint-based variable impedance using layer jamming," *IEEE Trans. Haptics*, vol. 12, no. 3, pp. 269–280, Jul. 2019.

[45] I. Choi, N. Corson, L. Peiros, E. W. Hawkes, S. Keller, and S. Follmer, "A soft, controllable, high force density linear brake utilizing layer jamming," *IEEE Robot. Autom. Lett.*, vol. 3, no. 1, pp. 450–457, Jan. 2018.

[46] Y. S. Narang, J. J. Vlassak, and R. D. Howe, "Mechanically versatile soft machines through laminar jamming," *Adv. Funct. Mater.*, vol. 28, no. 17, Feb. 2018, Art. no. 1707136.

[47] J. Song, Y. Chen, and G. Lu, "Axial crushing of thin-walled structures with origami patterns," *Thin-Walled Struct.*, vol. 54, pp. 65–71, May 2012.

[48] S. I. H. Shah, S. Bashir, M. Ashfaq, A. Altaf, and H. Rmili, "Lightweight and low-cost deployable origami antennas—A review," *IEEE Access*, vol. 9, pp. 86429–86448, 2021.

[49] W.-H. Chen *et al.*, "A programmably compliant origami mechanism for dynamically dexterous robots," *IEEE Robot. Autom. Lett.*, vol. 5, no. 2, pp. 2131–2137, Apr. 2020.

[50] W. Kim *et al.*, "Bioinspired dual-morphing stretchable origami," *Sci. Robot.*, vol. 4, no. 36, pp. 1–11, Nov. 2019.

[51] Y. Jiang, D. Chen, J. Que, Z. Liu, Z. Wang, and Y. Xu, "Soft robotic glove for hand rehabilitation based on a novel fabrication method," in *Proc. IEEE Int. Conf. Robot. Biomimetics (ROBIO)*, Dec. 2017, pp. 1–6.

[52] A. D. Marchese, R. K. Katzschmann, and R. Daniela, "A recipe for soft fluidic elastomer robots," *Soft Robot.*, vol. 2, no. 1, pp. 7–25, Mar. 2015.

[53] P. Polygerinos *et al.*, "Modeling of soft fiber-reinforced bending actuators," *IEEE Trans. Robot.*, vol. 31, no. 3, pp. 778–789, Jun. 2015.

[54] F. Connolly, P. Polygerinos, C. J. Walsh, and K. Bertoldi, "Mechanical programming of soft actuators by varying fiber angle," *Soft Robot.*, vol. 2, no. 1, pp. 26–32, May 2015.

[55] H. Wang *et al.*, "Fiber-reinforced soft robotic anthropomorphic finger," in *Proc. Int. Conf. Robot. Autom. Eng. (ICRAE)*, Aug. 2016, pp. 1–5.

[56] Z. Wang, P. Polygerinos, J. T. Overvelde, K. C. Galloway, K. Bertoldi, and C. J. Walsh, "Interaction forces of soft fiber reinforced bending actuators," *IEEE/ASME Trans. Mechatronics*, vol. 22, no. 2, pp. 717–727, Apr. 2017.

[57] H. Lamport and R. D. Eichhorn, "Design of a collapsible, lightweight 'iron lung' respirator," *Science*, vol. 108, no. 2802, pp. 288–289, Sep. 1948.

[58] C. H. Woollam, "The development of appartus for intermittent negative pressure respiration," *Anaesthesia*, vol. 31, no. 4, pp. 537–547, May 1976.

[59] M. G. Coulthard *et al.*, "Exovent: A study of a new negative-pressure ventilatory support device in healthy adults," *Anaesthesia*, vol. 76, no. 5, pp. 623–628, May 2021.

[60] P. T. Sancho, P. A. Gandarias, R. S. González, and A. A. Gurumeta, "Respiratory physiotherapy with vibration belts in the critical patient COVID-19 in the prone position," *Revista Española de Anestesiología y Reanimación*, vol. 67, no. 8, pp. 481–482, Oct. 2020.

[61] P. Banfi *et al.*, "Daytime noninvasive ventilatory support for patients with ventilatory pump failure: A narrative review," *Multidisciplinary Respiratory Med.*, vol. 14, Nov. 2019, Art. no. 38.